Since January 2020 Elsevier has created a COVID-19 resource centre with free information in English and Mandarin on the novel coronavirus COVID-19. The COVID-19 resource centre is hosted on Elsevier Connect, the company's public news and information website.

Biomedicine & Pharmacotherapy 155 (2022) 113666

Contents lists available at ScienceDirect

Biomedicine & Pharmacotherapy

journal homepage: www.elsevier.com/locate/biopha

Tanshinone IIA loaded bioactive nanoemulsion for alleviation of lipopolysaccharide induced acute lung injury via inhibition of endothelial glycocalyx shedding

Riham M. El-Moslemany [a,*], Amal H. El-Kamel [a], Eman A. Allam [b], Hoda M. Khalifa [c], Ahmed Hussein [d], Asmaa A. Ashour [a]

[a] Department of Pharmaceutics, Faculty of Pharmacy, Alexandria University, Alexandria 21521, Egypt
[b] Department of Medical Physiology, Faculty of Medicine, Alexandria University, Alexandria 21131, Egypt
[c] Department of Histology, Faculty of Medicine, Alexandria University, Alexandria 21131, Egypt
[d] Department of Biotechnology, Institute of Graduate Studies and Research, Alexandria University, Egypt

ARTICLE INFO

Keywords:
Bioactive nanoemulsion
Tanshinone IIA
Lung injury
Glycocalyx
Oxidative stress

ABSTRACT

Acute lung injury (ALI) and its more serious form; acute respiratory distress syndrome are major causes of COVID-19 related mortality. Finding new therapeutic targets for ALI is thus of great interest. This work aimed to prepare a biocompatible nanoformulation for effective pulmonary delivery of the herbal drug; tanshinone-IIA (TSIIA) for ALI management. A nanoemulsion (NE) formulation based on bioactive natural ingredients; rhamnolipid biosurfactant and tea-tree oil, was developed using a simple ultrasonication technique, optimized by varying oil concentration and surfactant:oil ratio. The selected TSIIA-NE formulation showed 105.7 nm diameter and a PDI ~ 0.3. EE exceeded 98 % with biphasic sustained drug release and good stability over 3-months. In-vivo efficacy was evaluated in lipopolysaccharide (LPS)-induced ALI model. TSIIA-NE (30 μg/kg) was administered once intratracheally 2 h after LPS instillation. Evaluation was performed 7days post-treatment. Pulmonary function assessment, inflammatory, oxidative stress and glycocalyx shedding markers analysis in addition to histopathological examination of lung tissue were performed. When compared to untreated rats, in-vivo efficacy study demonstrated 1.4 and 1.9-fold increases in tidal volume and minute respiratory volume, respectively, with 32 % drop in wet/dry lung weight ratio and improved levels of arterial blood gases. Lung histopathology and biochemical analysis of different biomarkers in tissue homogenate and bronchoalveolar lavage fluid indicated that treatment may ameliorate LPS-induced ALI symptoms thorough anti-oxidative, anti-inflammatory effects and inhibition of glycocalyx degradation. TSIIA-NE efficacy was superior to free medication and blank-NE. The enhanced efficacy of TSIIA bioactive nanoemulsion significantly suggests the pharmacotherapeutic potential of bioactive TSIIA-NE as a promising nanoplatform for ALI.

1. Introduction

The clinical and epidemiological features of coronavirus infection and COVID-19 related diseases are continuously reported. COVID19-related acute lung injury (ALI) and more dangerous acute respiratory distress syndrome (ARDS) are considered to be the main leading causes of COVID19-related mortality [1]. The underlying pathophysiological mechanisms of ALI/ARDS are complex. Pulmonary inflammatory response and oxidative stress are suggested to have an important role in ALI pathogenesis [2]. ALI and ARDS are usually characterized by increased pulmonary microvascular endothelial permeability leading to interstitial edema and alveolar collapse. Moreover, increased pulmonary

Abbreviations: ALI, Acute lung injury; ARDS, acute respiratory distress syndrome; BALF, bronchoalveolar lavage fluid; GPx, glutathione peroxidase; IL-10, interleukin 10; IL-17, interleukin 17; LPS, Lipopolysaccharide; MDA, malondialdehyde; MMP-9, metalloproteinase-9; NE, nanoemulsion; P407, Poloxamer 407; PG, Propylene glycol; Polydispersity index, Polydispersity index; RL, rhamnolipids; SDC-1, syndecan-1; SOD, superoxide dismutase; TNF-α, tumor necrosis factor-alpha; TSIIA, Tanshinone II A; TTO, tea tree oil; ZP, ζ-potential.

* Correspondence to: Department of Pharmaceutics, Faculty of Pharmacy, Alexandria University, 1 Khartoum Square, Azarita, Messalla Post Office, P.O.Box 21521, Alexandria, Egypt.
E-mail address: riham.elmoslemany@alexu.edu.eg (R.M. El-Moslemany).

https://doi.org/10.1016/j.biopha.2022.113666
Received 22 July 2022; Received in revised form 24 August 2022; Accepted 5 September 2022
Available online 12 September 2022

leukocytes' infiltration is usually present. These leukocytes initiate pulmonary inflammation and fibrosis as they produce pro-inflammatory mediators as well as profibrotic growth factors [3].

The glycocalyx is a gel-like layer that lines the luminal surface of the vascular endothelium. Endothelial glycocalyx layer existing on the surface of pulmonary vascular endothelium plays an important role in ALI/ARDS pathogenesis. It has a vital role in many physiological processes, including alveolar permeability, albumin exudation, pulmonary edema formation, and leukocyte adhesion [4]. The glycocalyx is composed of multiple glycoprotein complex substances, where syndecan-1 (SDC-1) is the most abundant component. Glycocalyx regulates vascular permeability as it functions as a negatively charged sieve limiting the movement of the negatively charged molecules (e.g. albumin) with establishment of an albumin gradient across the vessel wall. Therefore, the healthy glycocalyx regulates transvascular albumin and fluid flux (according to the starling forces that control tissue fluid formation) with prevention of tissue edema. When this layer is pathologically degraded in conditions such as ALI, it becomes thin and sparser which allows the plasma protein albumin and accordingly fluid to move freely across the vessel wall, resulting in formation of tissue edema [5].

Glycocalyx undergoes dynamic changes where enzymes are important key factor [6]. It is known that this enzymatic degradation is activated by reactive oxygen species (ROS) and inflammatory cytokines [7].

Matrix metalloproteinase-9 (MMP-9) is reported to be a syndecan degrading key enzyme [8]. SDC-1 degradation and shedding are considered to be an important indicator for severity, progression and aggravation of pulmonary diseases. Moreover, Parimon et al. [9] reported that SDC-1 may be involved in occurrence of pulmonary fibrosis and hence is considered as an important marker in lung injury prognosis and treatment [5]. According to all previously mentioned information, endothelial glycocalyx and its degradation may be an important therapeutic target in ALI.

There are no specific therapies for ALI with management relying on mechanical ventilation and supportive measures [10]. Since pulmonary inflammatory response and oxidative stress play an important role in ALI pathogenesis, therapy targeting their reduction could be an effective strategy.

Tanshinone IIA (TSIIA), a phenanthrenequinone derivative extracted from *Salvia miltiorrhiza* Bunge, is widely used in traditional Chinese herbal medicine. It has many pharmacological functions [11], such as anti-inflammatory and anti-oxidant properties [12]. Previous work has demonstrated its ability to alleviate ALI induced by lipopolysaccharide (LPS) either for prophylaxis [13] or treatment [14]. However, its therapeutic activity is limited owing to low aqueous solubility, poor bioavailability, short half-life, and extensive metabolism [15].

Several nano-technology based delivery systems were elaborated in the literature allowing for the formation of stable colloidal dispersion thus overcoming poor solubility and attempting to enhance bioavailability and protect the drug from metabolic enzymes [15–20]. Due to the hydrophobic nature of the drug, a lipid-based delivery system is expected to allow for increased drug loading and enhanced systemic bioavailability. Oil-in water (O/W) nanoemulsion system could be used as a suitable nanocarrier for effective TSIIA delivery. Nanoemulsions (NEs) have size ranges between 20 and 200 nm [21]. The large surface area offered by the small droplet size provide attractive physical properties and hence overcome both anatomical and physiological barriers thus enhancing bioavailability [22].

Since back to nature is the concept of recent and future pharmaceutical research based on phytomedicine and natural bioactive excipients, a nanoemulsion (NE) formulation for the delivery of TSIIA, based on biologically active ingredients assumed to be an attractive therapeutic option for ALI/ARDS. Several essential oils have been reported to reduce inflammation and improve lung function in ALI [23–25]. Of these, tea tree oil (TTO) has been extensively studied. TTO is the volatile essential oil derived from the Australian native plant *Melaleuca alternifolia*. It is used mainly for its antimicrobial, antioxidant and anti-inflammatory properties in addition to its anti-tumor and immune regulation effects [26]. It was previously shown that TTO inhalation exerts a strong anti-inflammatory effect on the immune system [27]. However, pharmaceutical application of TTO is limited due to its volatility, instability upon exposure to light or oxygen, hydrophobicity, and hence formulation difficulties [28]. Therefore, its formulation at the nanoscale provides an efficient method to enhance physical stability via protection against volatilization and environmental reactivity [28]. TTO was previously successfully formulated as NEs to enhance its stability [28,29].

In developing eco-friendly bioactive nanosystems, biosurfactants have emerged as a promising alternative both for the synthesis and stabilization of nanoparticles. Among the biosurfactants used, rhamnolipids (RL) have been widely used [30]. RL possess anti-inflammatory and anti-viral properties; hence several studies investigated their potential use as a strategy to treat or prevent COVID-19 disease [31].

Within this framework, the goal of this research was to formulate a biocompatible bioactive nanoformulation that would allow for successful pulmonary administration of tanshinone-IIA for the treatment of ALI. Up to our knowledge, a nanoemulsion system based on bioactive excipients; TTO and RL, was studied for effective pulmonary delivery of TSIIA for the first time. The prepared TSIIA-loaded NE was optimized for enhanced pharmaceutical attributes including colloidal properties, drug loading and drug release. Glycocalyx shedding, pulmonary inflammation and oxidative stress were the studied pathophysiological pathways to demonstrate the exact mechanism of action of the selected formulation for treatment of ALI.

2. Materials and methods

2.1. Materials

Tanshinone II A (purity 98 %) was purchased from Baoji Guokang Bio-Technology Co., Ltd (China). Rhamnolipids and tea tree oil were obtained from Sigma-Aldrich (USA). Poloxamer 407 (P407) was purchased from BASF Co. (Germany). Propylene glycol (PG) and ethanol were from ADWIC, El-Nasr Pharmaceutical Chemicals Co. (Egypt). Lipopolysaccharide (LPS) was extracted by the Department of Biotechnology, Institute of Graduate Studies and Research, Alexandria University, Egypt. Thiobarbituric acid (TBA), protease inhibitor cocktail and other reagents used in the in vivo study were obtained from Sigma-Aldrich (USA). All other chemicals and organic solvents were of analytical grade.

2.2. Preparation of blank and TSIIA-loaded nanoemulsion (TSIIA-NE)

A high-energy ultrasonication technique was used to prepare TSIIA loaded O/W NEs as previously described with some modifications [32,33]. The effect of different formulation variables including oil concentration (3 %, 5 % and 8 %) and surfactant:oil ratio (1:1, 2:1 and 1:2) was investigated (Table 1). TTO was selected as the oily phase, P407 as the surfactant and RL/ PG as the cosurfactants. The oil and cosurfactants were mixed, then added drop wise to the aqueous phase (water containing P407) under continuous magnetic stirring at 800 rpm for 5 min to form a coarse emulsion. To obtain a nano-dispersion, sonication for 10 min was carried out using a probe sonicator (Bandelin sonopuls, Germany) at 60 % amplitude in an ice bath to avoid any loss of the volatile essential oil. For preparation of TSIIA-NE, a 1.25 mg of TSIIA is added to the oily phase and the same procedures were applied.

2.3. In vitro characterization

2.3.1. Colloidal properties

Average particle size (PS), polydispersity index (PDI) and ζ-potential (ZP) of NE formulations were analyzed using Malvern Zetasizer (Nano-ZS Series DTS 1060, Malvern Instruments, Worcestershire, UK).

Table 1
Formulation code, composition and physicochemical properties of different prepared TSIIA-NEs.

Formulation code	Oil (% w/v)	SAA: Oil ratio	Size (nm)	PDI	Zeta potential (mV)	% EE
F1	3	1:2	145.5 ± 1.3	0.26 ± 0.01	-31.3 ± 1.2	94.1 % ± 1.02
F2	3	1:1	100.5 ± 0.9	0.22 ± 0.01	-29.2 ± 1.5	94.5 % ± 0.84
F3	3	2:1	63.4 ± 0.1	0.25 ± 0.01	-27.1 ± 0.9	94.9 % ± 0.95
F4	5	1:2	148.1 ± 1.6	0.22 ± 0.02	-34.4 ± 1.7	96.3 % ± 1.28
F5	5	1:1	101.2 ± 1.2	0.26 ± 0.01	-28.3 ± 2.0	96.6 % ± 1.55
F6	5	2:1	65.6 ± 0.8	0.30 ± 0.02	-27.8 ± 0.8	96.0 % ± 0.72
F7	8	1:2	150.0 ± 0.9	0.11 ± 0.01	-35.9 ± 2.1	98.0 % ± 0.43
F8	8	1:1	105.7 ± 0.9	0.31 ± 0.02	-29.5 ± 1.8	98.4 % ± 1.32
F9	8	2:1	71.9 ± 1.4	0.29 ± 0.01	-26.1 ± 1.0	98.6 % ± 0.62

Propylene glycol, 100 mg was added to all formulations.
In all formulations, poloxamer 407: rhamnolipid ratio was 3:2.
Values represent mean ± SD, n = 3.

Measurements were done at a fixed angle at 25 °C using a 4 mW He–Ne laser at 633 nm. Formulations were adequately diluted with deionized water and measured in triplicates.

2.3.2. Morphological examination

The morphology of the selected NE formulation was investigated following staining with uranyl acetate by transmission electron microscope (TEM) (model JEM-100CX (JEOL, Japan). The formulation was sprayed onto copper grids before analysis. Shots were taken at × 15K magnification.

2.3.3. Entrapment efficiency determination (EE%)

TSIIA %EE in the prepared NEs was determined by filtration/ultracentrifugation technique using (Sartorius™ Vivaspin6™, MWCO 100,000) to separate free unentrapped TSIIA following centrifugation (Sigma 3–30KS, Sigma Laborzentrifugen GmbH, Germany) for 30 min at 6000 rpm at 4 °C [11]. Prior to centrifugation, the formulations were 4-fold diluted with deionized water. The concentration of unentrapped TSIIA in the filtrate was determined spectrophotometrically (UV-160A double beam spectrophotometer, Agilent tech., USA) at λ_{max} 270 nm. The % EE was calculated using the following equation:

$$\% \quad EE = \frac{(Ci - Cf)}{Ci} \times 100 \qquad (1)$$

where C_i is the initial drug content and C_f is the free drug in the supernatant.

2.3.4. In vitro TSIIA release

Release of TSIIA from the selected NE formulation was investigated by the dialysis method [15]. TSIIA-NE (1 ml equivalent to 250 μg TSIIA) was placed in presoaked dialysis bags (VISKING® dialysis tubing MWCO 12,000–14,000), which were then immersed in 20 ml release medium (ethanol: water, 1:1) maintaining sink conditions. The flasks were maintained in a thermostatically controlled shaking water-bath at 37 °C, 100 rpm. At different time intervals (1–24 h), samples (1 ml) were withdrawn and replaced with fresh medium. TSIIA concentration was determined spectrophotometrically at 270 nm. The experiment was done in triplicate.

The kinetics of release of TSIIA from NE was evaluated using model dependent methods calculated by the Excel add in; DDsolver [34].

2.3.5. Storage stability

TSIIA-NE stability upon storage was conducted at 4 °C for 3 months. Changes in particle size and entrapment efficiency were determined at 1, 2 and 3 months.

2.4. In vivo studies

2.4.1. Animals and ethical statement

Thirty-five male Wistar albino rats (160–180 g; average 8–10 weeks-old) were purchased from the Animal House of Medical Physiology Department, Faculty of Medicine, Alexandria University. Animals were housed in plastic cages (5 per cage) in normal room temperature (25 ± 2 °C) and 12 h light: dark cycle, with ad libitum access to food and water. All experimental procedures were performed in accordance with the Guide for the Care and Use of Laboratory Animals. The study proposal was approved by the Research Ethics Committee of Faculty of Medicine, Alexandria University (IRB code 00012098-FWA: No. 00018699; membership in International Council of Laboratory Animal Science Organization, ICLAS).

2.4.2. LPS extraction and purification

LPS was extracted from E.coli by hot phenol-water method as previously described with some modifications [35]. Detailed extraction and purification procedure is provided in Supplementary material.

2.4.3. Induction of ALI and experimental groups

One week was allowed for acclimatization prior to the experiment. Then, induction of ALI was performed in 28 rats by intratracheal instillation of 0.2 ml LPS in PBS (5 mg/kg) [36]. The other 7 rats received an equal volume of PBS and served as a negative control group. Two hours later, LPS injected rats were further randomly divided into 4 groups; untreated control (positive control), TSIIA suspension in 1:9 (PEG 400: normal saline), blank NE (NE-F8) and TSIIA-loaded NE (TSIIA-NE-F8). Rats were intratracheally instilled as follows: TSIIA suspension and TSIIA-NE-F8 groups received a single dose equivalent to 30 μg/kg TSIIA, while NE-F8 and the negative or positive control groups received equal volumes of NE-F8 and normal saline, respectively. Pulmonary functions were assessed 7 days following treatment then animals were anesthetized and sacrificed for specimen collection [37].

2.4.4. Lung assessment

2.4.4.1. Pulmonary function. Using a Power lab digital data acquisition system, tidal volume and minute respiratory volume were measured to assess lung condition and function. The parameters were recorded using a pneumothorax MLT1L (Lab chart 8, AD instruments, Castle Hill, NSW, Australia) where P1 channel end was connected to the outlet of the NP/Whole Body Plethysmography (WBP) [38].

After performing pulmonary functions, rats were anesthetized to obtain arterial blood samples, bronchoalveolar lavage fluid (BALF) and both lungs were excised. The left lung was used for histopathological examination. One lobe from the right lung was stored at − 80 °C for further biochemical measurements. The remainder was used to calculate wet/dry lung weight ration.

2.4.4.2. Wet/dry lung weight ratio. To calculate the wet/dry (W/D) lung weight ratio, excised lung tissues were weighed immediately to obtain the wet lung weight. Then they were reweighed after drying in an oven at 80 °C for 48 h to obtain the dry lung weight. The (W/D) ratio was used as an indicator for pulmonary edema [39].

2.4.4.3. Arterial blood gases (PaO_2/FiO_2). Following anesthesia, arterial blood samples were collected from the abdominal aorta in heparinized syringes. PaO_2 which is the partial pressure of oxygen in arterial blood was then measured using arterial blood gas analyzer (Gem® Premier

3000, Instrumentation Laboratory, USA). Then, PaO_2/FiO_2 ratio was calculated. FiO_2 is the fraction of oxygen in the inspired air and was considered as 0.21 [40].

2.4.4.4. BALF collection and inflammatory cell counting. In order to make the lavage forced to the left lung, we did suture clamps on the right main bronchus. After that, 3 ml ice-cold PBS was injected into the left lung using a tracheal cannula under anesthesia. Flushing the lung with PBS was done three times. The collected BALF was then centrifuged for 10 min at 600 *g* at 4 °C. Following centrifugation, the supernatant was stored at − 80 °C for further biochemical assessment. The remaining cell pellet was re-suspended in 0.5 ml PBS. Then the samples were smeared and stained for microscopical examination. Three main types of leukocytes; macrophages, lymphocytes and neutrophils were counted by light microscopic imaging using × 40 object lens. The numbers were calculated in 5 different fields using computer program MAtLAB software (image J, the mathworks, inc., USA).

2.4.4.5. Lung tissue homogenization and biochemical analysis. Frozen lung tissues were homogenized in PBS containing protease inhibitors cocktail. The produced homogenate was centrifuged at 2000 *g* for 15 min at 4 °C. The resultant supernatant was collected for measurement of total protein content by Lowry method [41]. Then, it was used for biochemical measurements.

2.4.4.5.1. Assessment of inflammatory markers. The levels tumor necrosis factor-alpha (TNF-α) (Cat#MBS1754207, MyBiosource, USA), interleukin 10 (IL 10) (Cat# MBS2036296, MyBiosource, USA) and interleukin 17 (IL 17) (Cat# MBS211293, MyBiosource, USA) in lung tissue homogenates were determined using ELISA method according to the manufacturer's instructions.

2.4.4.5.2. Assessment of oxidant-antioxidant balance. The oxidative stress marker: malondialdehyde (MDA) level was measured using thiobarbituric acid reaction colorimetric method and its concentration was represented in the form of nmol/mg protein [42]. Regarding antioxidant enzymes in lung tissue, the activities of superoxide dismutase (SOD) (EC 1.15.1.1) and glutathione peroxidase (GPx) (GP 2524, Biodiagnostic, Egypt) were determined spectrophotometrically as previously described [43,44], and the results expressed as U/mg tissue protein.

2.4.4.5.3. Assessment of glycocalyx shedding markers. Syndecan-1 (SDC-1) was measured using ELISA technique (Cat# MBS2512881, MyBiosource, USA) following the manufacturer's instructions both in lung tissue homogenate and supernatant of BALF and the results were expressed as ng/mg tissue protein & ng/ml respectively. Moreover, matrix metalloproteinase-9 (MMP-9) (Cat# MBS722532, MyBiosource, USA) was measured in lung tissue homogenate by ELISA method according to the manufacturer's instructions and the results were expressed as pg/mg tissue protein.

2.4.4.6. Pulmonary histopathological analysis. Lung tissue samples were fixed in 10 % formalin saline. Each specimen was then processed to obtain 6-μm thick paraffin sections to be stained with H&E stain. Images were viewed and recorded using a light microscope (Olympus America Inc., USA) – equipped with Spot digital camera with numerical aperture of a high resolution (16-bit digital camera (1280 × 1024) pixels).

2.5. Statistical analysis

The results are presented as Mean ± SD. All statistical analysis was performed using IBM SPSS software (package version 21, 2012). Statistical significance was determined using one-way analysis of variance (ANOVA) followed by Duncan post-hoc test for pair-wise comparisons. Differences were considered significant when $p \leq 0.05$.

3. Results and discussion

3.1. Preparation and optimization of TSIIA-NE

In the present study, TSIIA-NE was prepared for the first time using natural biologically active ingredients. TTO was selected as the oily phase with the SAA/Co-SAA system, P407/ RL in the ratio 2:3. A volume of PG (100 mg) was added to all formulations as a part of co-SAA system. For optimization, oil concentration was varied (3–8 % w/v of the final volume of NE). In addition, different surfactant: oil ratios were investigated. The effect of these formulation variables on the colloidal properties of the prepared NEs as well as TSIIA % EE are presented in Table 1.

The mean droplet size of the tested NEs ranged from 63.4 ± 0.1 to 150 ± 0.9 nm. The smallest size was attained by F3 with the lowest oil content (3 % w/v) and highest SAA: oil ratio (2:1). The results reflect that the increase in SAA: oil ratio at a constant oil concentration brought about a highly significant decrease in droplet size of the NE as obvious for the three oil concentrations tested ($p \leq 0.001$). This could be due to the increased population of the surfactant molecules at the droplet interface [45]. On the other hand, for similar SAA: oil ratio, no significant change in droplet size was observed upon increasing oil content due to the proportional increase in SAA concentration ($p > 0.05$). All the formulations showed low values of PDI (0.11 ± 0.01 to 0.31 ± 0.02) indicating droplet size uniformity. The results obtained agreed with the size range reported previously in the literature for NE [19,46,47].

The developed NE formulations showed a ZP ranging from − 26.1 ± 1 to − 35.9 ± 2.1 (Table 1). This relatively high negative ZP is expected to enhance formulation stability. It is well reported that ZP values > 20 mV are sufficient to prevent the coalescence of oil droplets in the NE formulations thus confirming their colloidal stability [28]. The high negative charge existing on the prepared NEs could be explained by the presence of anionic groups of fatty acids in the TTO, glycol part of P407 [48] in addition to the anionic nature of RL [45,49]. Also, ZP values slightly decreased with decreasing droplet size. This is in agreement with the results previously described by Al-Sakkaf et al. [45]. This was attributed to a decrease in charge density as the emulsion droplet shrinks leading to a lower ZP [45].

TSIIA showed high entrapment efficiency exceeding 94 % for all tested NE formulations. %EE values varied from 94.1 ± 1.02 to 98.6 ± 0.62%. It can be deduced from the results that increasing SAA: oil ratio at a constant oil concentration resulted in a slight insignificant increase ($P > 0.05$) in %EE. On the other hand, increasing oil concentration from 3 % to 8 % at constant SAA: oil ratio brought about a gradual significant increase in TSIIA % EE ($p \leq 0.05$). This could be attributed to the high lipophilicity of the drug and hence increased solubilization with increasing oil concentration, reflecting the high solubility of TSIIA in the selected oil. These findings corroborated with what was previously reported for the increase in % EE of the hydrophobic drug quercetin in NE by increasing oil content while keeping the SAA constant [50].

Based on the aforementioned results and due to the slight differences in colloidal properties and %EE among different formulations tested, F8 with 8 % oil and 1:1 SAA: oil ratio was selected as an optimum formulation for further in vitro and in vivo characterization. The selection was based on its high oil content which is intended to achieve a better in vivo performance. Despite the smaller particle size observed for F9, F8 was preferred due to its lower SAA concentration.

3.2. Morphology

Macroscopical (Fig. 1A) and TEM imaging (Fig. 1B) of the selected formulation F8 displayed the typical appearance of an o/w emulsion with morphological characteristics matching with those described earlier [19,28,51]. The NE appeared as non-aggregated, almost spherical shaped globules and homogenous size distribution (Fig. 1B). The

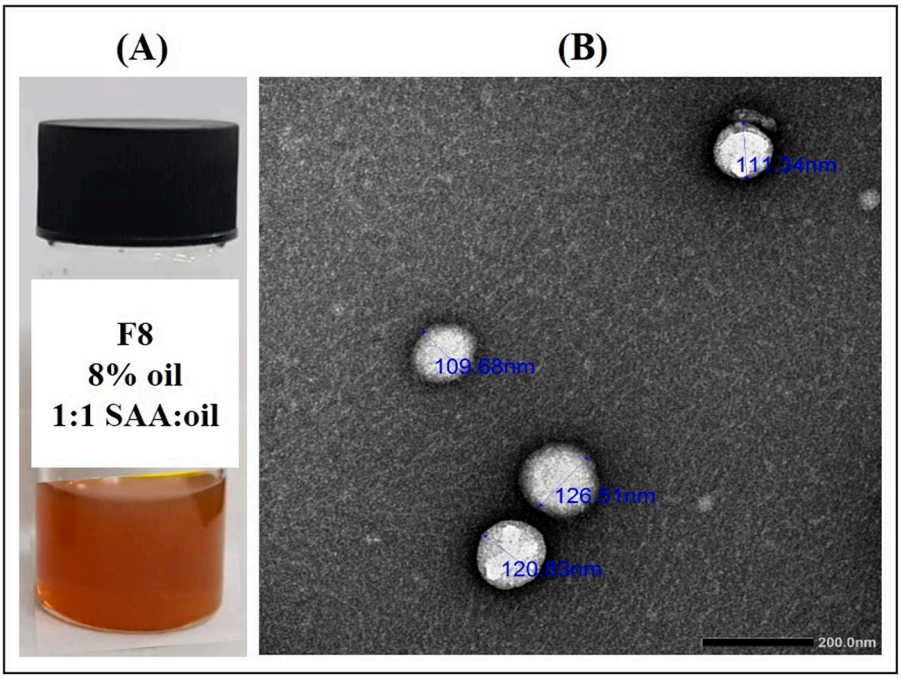

Fig. 1. (A) Macroscopical appearance of selected TSIIA-NE-F8 and **(B)** Transmission Electron Micrograph of TSIIA-NE-F8 at magnification × 30 K; Scale bar represents 200 nm.

higher contrast at the oil/water interface could be attributed to the affinity of uranyl acetate used for negative staining to interface components as was previously reported [52]. Furthermore, the observed sizes from TEM were near the hydrodynamic diameter measured by the dynamic light scattering.

3.3. In vitro drug release

In vitro drug release profile of TSIIA suspension and the selected TSIIA-NE-F8 is shown in Fig. 2. TSIIA suspension showed a relatively high burst release ~ 40 % after 1 h of the release study with almost 100 % released after 7 h. On the contrary, TSIIA-NE-F8 exhibited a significantly lower % cumulative release with only ~ 75 % released after 24 h suggesting the ability of the prepared NE to permit for a sustained TSIIA release. Also, TSIIA loading into NE resulted in a significant 50 % reduction in burst release ($p \leq 0.05$). The burst release of TSIIA from NE may be attributed to the unentrapped drug adsorbed on the surface of oil droplets rather than being incorporated in core of oily globules. The observed controlled release profile of TSIIA is consistent with previous studies in which a sustained drug release from NEs was attributed to the efficient solubilization and encapsulation of the drug in the oily phase of NE [51].

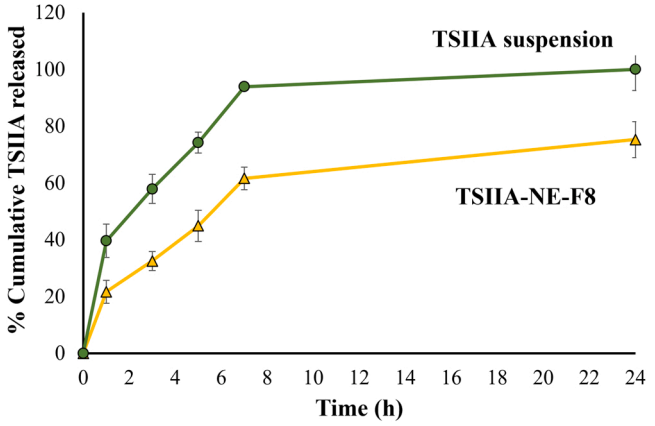

Fig. 2. Release profiles of TSIIA-NE-F8 versus TSIIA suspension at 37 °C. Data presented as means ± SD (n = 3).

The drug release mechanism of TSIIA-NE-F8 was determined by fitting to different release kinetics models; the coefficient of determination was in the following order: 0.219, 0.866, 0.894, 0.955 and 0.804 for zero-order, first-order, Higuchi, Korsmeyer-Peppas and Hixson Crowell models, respectively. It was observed that R^2 for TSIIA-NE-F8 fitted best with Korsmeyer-Peppas model (0.955) where the release exponent value (n) was ≤ 0.5, indicating that drug release follows a Fickian diffusion manner [48].

3.4. Storage stability

Table 2 shows the effect of storage on the colloidal properties as well as TSIIA % EE for TSIIA-NE-F8 at 4 °C for 3 months. Visual inspection of the formulation indicated that the prepared formulation was stable with no detected signs of phase separation or drug precipitation upon storage. The negligible variations in the evaluated physicochemical parameters verified the stability of the formulation for 3 months at 4 °C. Similar results were reported previously for the long-term storage stability of the NE systems stabilized by either P407 [48] or RL [49]. The stability of NE could be attributed to the ability of SAA molecules to adsorb on the surface of oil droplets via their hydrophobic parts, stabilizing them against coalescence [48,49].

Table 2
Storage stability data of TSIIA-NE-F8 at 4 °C for 3 months (n = 3).

Time (months)	Droplet size (nm)	PDI	Zeta potential (mV)	TSIIA % EE
0	105.7 ± 0.87	0.31 ± 0.02	-26.1 ± 1.0	98.4 ± 1.3
1	102 ± 0.6	0.27 ± 0.01	- 26.7 ± 0.8	98.1 ± 2.4
2	101 ± 1.2	0.30 ± 0.004	- 25.8 ± 0.6	98.0 ± 1.2
3	104 ± 0.73	0.29 ± 0.006	- 26.3 ± 0.4	98.6 ± 2.1

3.5. In vivo efficacy

An LPS-induced ALI model was used for pharmacodynamic evaluation of TSIIA-NE-F8 compared to the appropriate controls. LPS has been widely considered as an effective strategy to establish ALI animal models. It targets mainly the alveolar epithelium, activates acute and aggressive leukocyte migration and oxygen free radicals production in the pulmonary tissue. Moreover, LPS affects type II alveolar cells that produce the surfactant as LPS interacts with surfactant-specific receptors leading to their inactivation [53]. This eventually results in ALI especially when used by intratracheal instillation [54]. Moreover, intratracheal instillation mimics the clinical scenario of respiratory acquired infections. A single dose of different treatments was administered 2 h after LPS instillation followed by a seven day period before evaluation to enable them to exert their action thus allowing for discrimination [37].

3.5.1. Wet to dry lung weight ratio

As shown in Fig. 3A, the W/D weight ratio revealed an 85 % increase in the positive control versus the negative control group indicating a state of pulmonary edema and inflammation [55]. This was reflected on pulmonary function as shown by the significant decrease in tidal volume (TV) and minute respiratory volume (MRV) by 70 % and 83 %, respectively ($p \leq 0.05$) (Fig. 3B and C). Representative tracings of airway flow and tidal volume are shown in Fig. 3D. A significant reduction in W/D weight ratio with a subsequent significant increase in TV and MRV (Figs. 3B and 3C) were observed following treatment with TSIIA suspension and blank NE. Maximum improvement was observed for the TSIIA-NE-F8 treated group reaching 32 % reduction in W/D weight ratio and 1.4 and 1.9 fold increase in TV and MRV, respectively, when compared to positive control group.

3.5.2. Arterial blood gases

Blood gas analysis (Fig. 4) revealed successful induction of ALI. A significant reduction in PaO_2 and PaO_2/FIO_2 following LPS instillation was observed compared to the negative control group. Reduced PaO_2/FIO_2 is a clinical diagnostic standard of ALI [56]. Different treatments resulted in evident improvement in both parameters with the significant improvement results recorded for TSIIA-NE-F8.

The improvement observed in pulmonary function, W/D lung weight ratio and arterial blood gases after administration of TSIIA-NE-F8 reflected the protective effects TSIIA [14,37,57] and the NE bioactive excipients; RL and TTO [58,59], against ALI. The noticeable improvement observed for TSIIA-NE-F8 could be due to the combined efficacy of TSIIA and bioactive NE. The possible mechanism will be discussed later throughout the following sections.

3.5.3. BALF inflammatory leukocytic count changes

Differential leukocytic counts in BALF were assessed to determine the anti-inflammatory activities of TSIIA suspension, NE-F8 and TSIIA-NE-F8 compared to negative and positive control groups (Fig. 5A–C). Negative control group BALF samples revealed low levels of macrophages, lymphocytes and neutrophils. On the other hand, positive control group samples showed marked significant increase in cell counts ($p \leq 0.05$). Following treatment, evident changes in cellular composition were observed in all treated groups. TSIIA-NE-F8 treated group revealed predominance of macrophages while lymphocytes and neutrophils were reduced to a level comparable to the negative control group ($p > 0.05$). The predominance of macrophages following treatment could be explained by the dual role they play as they exert both proinflammatory and anti-inflammatory effects based on the microenvironment in different pathological stages [60]. Although, TSIIA suspension and NE-F8 treated groups exhibited significantly lower lymphocyte and neutrophils counts compared to the positive control

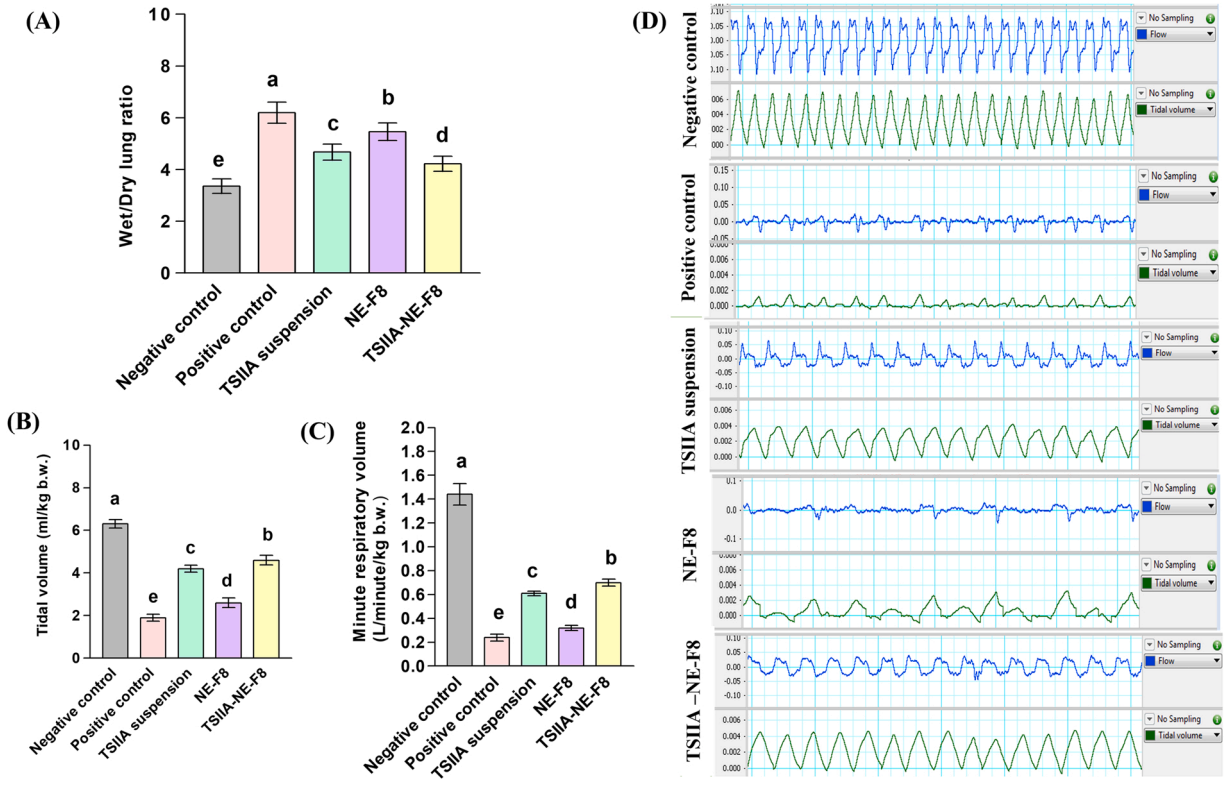

Fig. 3. Effect of different treatments on; **(A)** Wet/Dry lung weight ratio, **(B)** Tidal volume and **(C)** Minute respiratory volume following a single intratracheal dose in an LPS induced ALI rat model. Data expressed as mean ± SD (n = 7). Data analyzed using one-way ANOVA followed by post hoc test (Duncan) for group comparisons. Means of similar symbols were statistically insignificant: a > b > c > d > e ($p \leq 0.05$). **(D)** Representative tracing of airway flow (upper panel) and tidal volume (lower panel) following treatment compared to negative and positive controls.

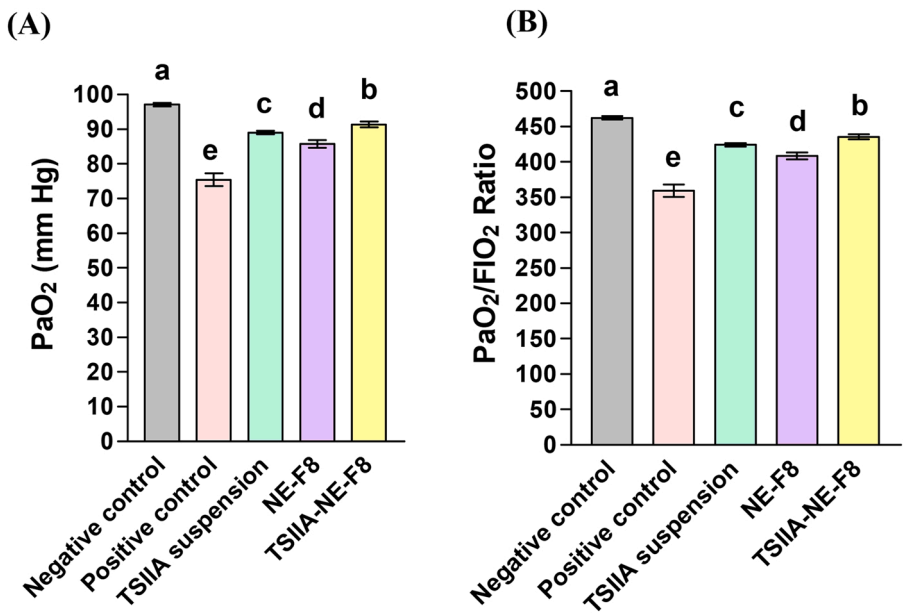

Fig. 4. Effect of different treatments on arterial blood gases following a single intratracheal dose in an LPS induced ALI rat model; **(A)** Partial pressure of oxygen in arterial blood (PaO_2) and **(B)** PaO_2/FiO_2 ratio. Data expressed as mean ± SD (n = 7). Data analyzed using one-way ANOVA followed by post hoc test (Duncan) for group comparisons. Means of similar symbols were statistically insignificant: a > b > c > d > e ($p \leq 0.05$).

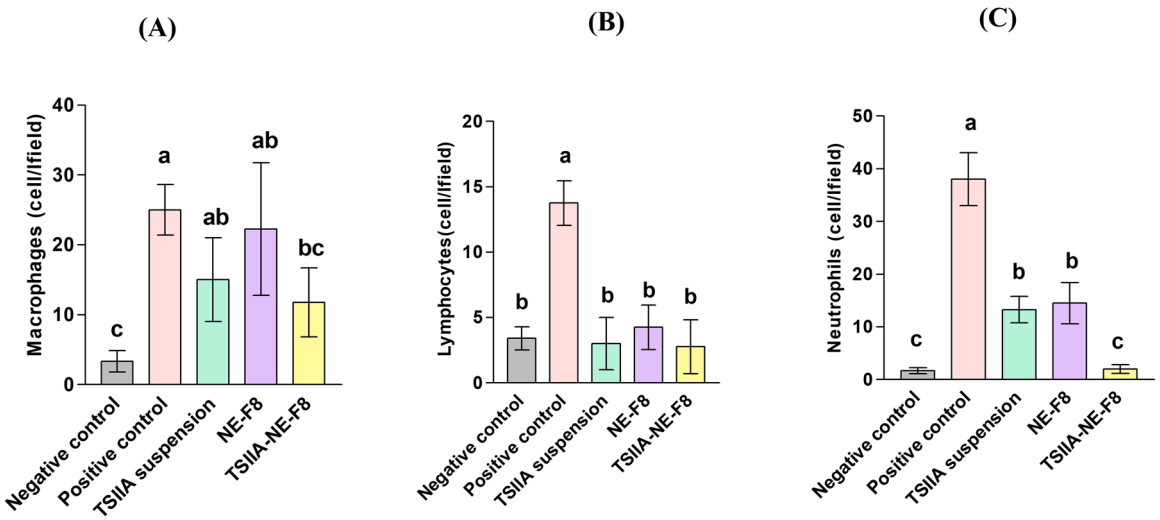

Fig. 5. (A–C) Effect of different formulations and TSIIA suspension on leukocytic count in bronchoalveolar lavage for all study groups; **(A)** Macrophages, **(B)** Lymphocytes, and **(C)** Neutrophils. Data were expressed as means ± SD (n = 7). Data were analyzed using one-way ANOVA followed by post hoc test (Duncan) for group comparisons. Means of similar symbols were statistically insignificant: a > b > c ($p \leq 0.05$).

($p \leq 0.05$) but the neutrophils count was still significantly higher than the negative control and TSIIA-NE-F8 treated groups ($p \leq 0.05$).

3.5.4. Changes in pulmonary inflammatory markers

Challenging the lung with various insults including LPS is known to initiate several inflammatory responses displaying cytotoxic effects on lung tissues. Following ALI onset, inflammatory cells are recruited into the lungs releasing inflammatory cytokines, reactive oxygen species (ROS), cationic peptides, and hydrolytic proteinases [14]. The released pro-inflammatory cytokines including TNF-α and IL-1β play a key role in ALI progression [14]. In this respect, following LPS intratracheal administration severe pulmonary inflammatory changes were observed as evidenced by the significant elevation in the levels of both TNF-α and IL-17 (by 3.1 and 1.5-folds, respectively) together with the significant 80 % decrease in the level of the anti-inflammatory marker; IL-10 compared to the negative control group ($p \leq 0.05$) (Fig. 6). Different treatments significantly depleted the pro-inflammatory cytokines with significant increase in IL-10 compared to the positive control group ($p \leq 0.05$). TSIIA suspension group revealed 49 % and 40 % decrease in the levels of both TNF-α and IL-17, respectively, with elevation in the level of IL-10 by ~ 1.7-folds versus the positive control group ($p \leq 0.05$) (Fig. 6). This was due to the reported anti-inflammatory action of TSIIA which has been previously described in similar ALI models [14,37,61]. This effect was also described in different models other than ALI where TSIIA elevated the level of the anti-inflammatory cytokine IL-10 following liver injury [62]. Also, Yan et al. [63] reported a decrease in the inflammatory IL-17 level in an autoimmune encephalomyelitis rat model.

Regarding NE-F8 group, the levels of both TNF-α and IL-17 were significantly decreased by 23 % and 29.3 %, respectively, while the level

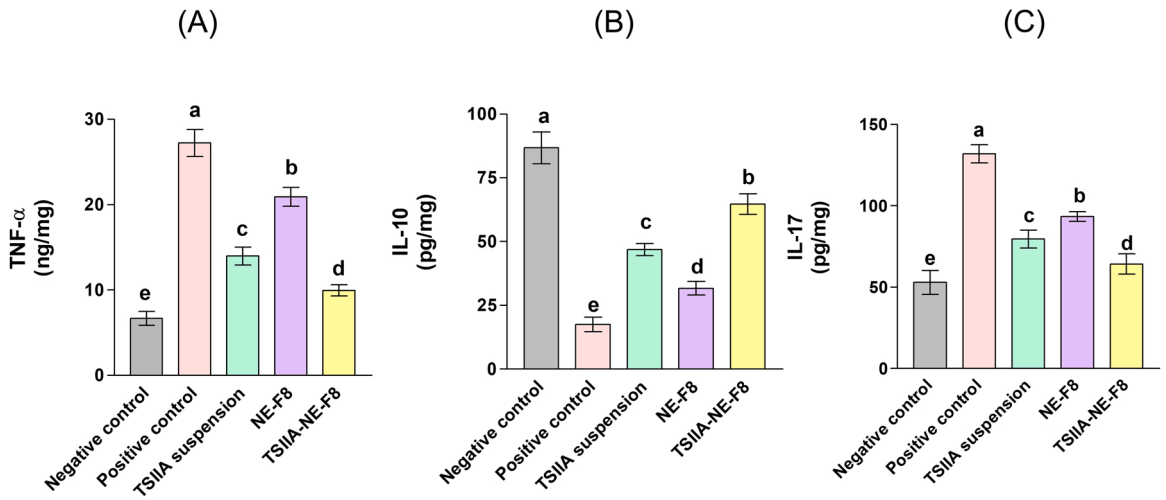

Fig. 6. Evaluation of various lung inflammatory markers;(A) Lung Tumor necrosis factor-alpha (TNF-α), (B) Lung interleukin-10 (IL-10), (C) Lung interleukin-17 (IL-17) following a single intratracheal administration of TSIIA-NE-F8 equivalent to 30 μg/kg compared to suitable controls. Values were expressed as mean ± SD (n = 7). Data were analyzed using one-way ANOVA followed by Post Hoc test (Duncan) for group comparisons. Means of similar symbols are statistically insignificant, a > b > c > d > e ($p \leq 0.05$).

of IL-10 was significantly increased by 81 % when compared with positive control group ($p \leq 0.05$) (Fig. 6). This was ascribed to the pronounced anti-inflammatory activities of the used bioactive ingredients; TTO and RL [64–67].

Interestingly, the administration of TSIIA-NE-F8 resulted in further significant improvement in the values of the tested markers (63.3 % and 52 % decrease in TNF-α and IL-17, respectively, and ~ 2.7-folds increase in IL-10) when compared to the positive control ($p \leq 0.05$). The previous findings reflect the important role of bioactive ingredients (TTO and RL) used in preparation of the NE system in augmenting the anti-inflammatory activity of TSIIA.

The levels of proinflammatory and anti-inflammatory cytokines is supported by the observed BALF inflammatory cell count changes where maximum reduction in neutrophil counts was also achieved by TSIIA-NE-F8.

3.5.5. *Changes in pulmonary oxidative stress markers*

It is widely addressed that oxidative stress is one of the key factors contributing to ALI [68]. It is caused by an imbalance between the generation and elimination of ROS and leads to the formation of products, such as malondialdehyde (MDA) with a decrease in expression of antioxidant enzymes [69]. Oxidative stress markers were evaluated in the current work and the results shown in Fig. 7. A significant disturbance in oxidant- antioxidant balance in favor of oxidative stress was observed in the positive control group. LPS instillation resulted in a significant increase in lung MDA level by ~ 2.4-folds along with a significant decrease in the levels of the antioxidant enzymes; SOD and GPx (75.5 % and 57 % decrease, respectively), compared to the negative control rats ($p \leq 0.05$). This is attributed to the well documented ability of LPS to induce oxidative stress mediated tissue damage [69–71].

Intratracheal administration of different formulations significantly upregulated SOD and GPx activity, with marked reduction in MDA level compared to the positive control group ($p \leq 0.05$). The observed improvement in the levels of the tested markers for TSIIA suspension group (42 % decrease in MDA with 160 % and 104 % increase in SOD and GPx, respectively versus positive control) was mainly due to its reported antioxidant properties [72]. The drug not only effectively trap the generated ROS, but also up-regulate the nuclear factor erythroid 2–related factor 2 which regulates cellular resistance to oxidants as well as antioxidant enzyme activities [72]. Concerning NE-F8, only 23 %

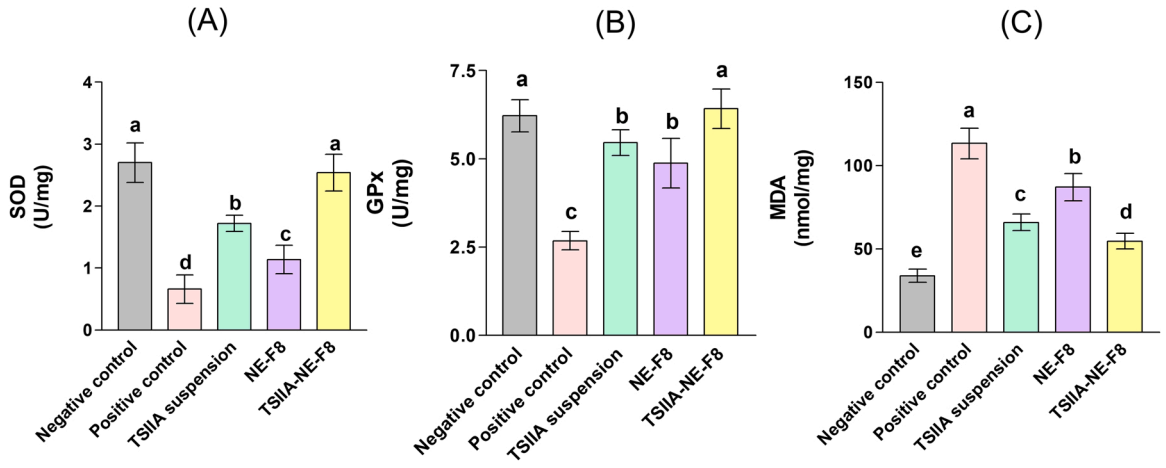

Fig. 7. Level of different lung oxidative stress markers; (A) Superoxide dismutase (SOD), Glutathione peroxidase (GPx) and malondialdehyde (MDA) following a single intratracheal administration of TSIIA-NE-F8 equivalent to 30 μg/kg compared to suitable controls. Values were expressed as mean ± SD (n = 7). Data were analyzed using one-way ANOVA followed by Post Hoc test (Duncan) for group comparisons. Means of similar symbols are statistically insignificant, a > b > c > d > e ($p \leq 0.05$).

reduction in MDA along with 73 % and 82 % increase in SOD and GPx, respectively versus positive control was achieved. The detected alleviation of the induced oxidative stress was attributed to the previously described anti-oxidant activities of the bioactive ingredients used; TTO and RL [73,74]. Despite the significant improvement achieved by TSIIA suspension and NE-F8 compared to the positive control group ($p \leq 0.05$), they were still significantly inferior to TSIIA-NE-F8 (Fig. 7). The latter accomplished ~ 50 % reduction in MDA with restoration of the normal levels of both lung SOD and GPx as evidenced by the insignificant difference compared to the negative control ($p > 0.05$).

3.5.6. Changes in glycocalyx shedding

Increased permeability of the pulmonary capillary endothelium is one of the important pathological mechanisms of ALI as it leads to pulmonary interstitial edema and exudate formation [75]. This increased permeability is closely related to the endothelial glycocalyx degradation [76]. Recently, protection against glycocalyx degradation and shedding is considered a key factor and an important therapeutic target in treatment of ALI [5,77]. In this context, the possible protective effect of different formulations through maintaining glycocalyx integrity in LPS-induced ALI rat model was investigated in the current work as a new therapeutic target for TSIIA. The results are shown in Fig. 8.

Results revealed that LPS instillation led to increased pulmonary glycocalyx shedding as was evident by the significant decrease in SDC-1 pulmonary level by 75 % (Fig. 8 A) together with consequent significant increase in its level in BALF by 3-folds (Fig. 8 B) compared to the negative control group ($p \leq 0.05$). Moreover, the expression of the glycocalyx degrading enzyme (MMP-9) was significantly elevated in the positive control group by 4.2-folds versus the negative control one ($P \leq 0.05$) (Fig. 8 C). Our results are in agreement with Zhang et al. [6] and Liu et al. [78] who reported increased glycocalyx shedding in LPS-induced ALI in an animal model.

Intratracheal administration of different treatments to diseased rats resulted in varying degrees of improvement. TSIIA suspension group brought about 1.2-fold increase in lung SDC-1 (Fig. 8 A) with 36.5 % and 52 % decrease in BALF SDC-1 and MMP-9, respectively (Fig. 8 B and C). NE-F8 effect on glycocalyx shedding was inferior to TSIIA suspension causing only 0.3 fold increase in lung SDC-1 (Fig. 8 A) with 18 % and 28 % decrease in BALF SDC-1 and MMP-9, respectively (Fig. 8 B and C). Maximum improvement was achieved by TSIIA-NE-F8 (1.9 fold increase in lung SDC-1 (Fig. 8 A), 53.7 % decrease in BALF SDC-1 (Fig. 8 B) and 68 % decrease MMP-9 (Fig. 8 C)). The effect of TSIIA, TTO and RL in inhibition of glycocalyx degradation could be explained by their pronounced anti-inflammatory [14,37,61,64–67] and antioxidant [72–74] properties. It was found that inflammation can induce the formation and release of glycocalyx degradation enzymes especially MMP-9 [79] and also an incomplete glycocalyx can aggravate the pulmonary inflammatory reaction resulting in a vicious circle leading to continuous lung injury [80]. Additionally, it was previously stated that oxidation/antioxidant imbalance is an important key in glycocalyx degradation [81]. The surpassing ability of TSIIA-NE-F8 to cause the maximum increase in SDC-1 level in lung tissue with subsequent reduction in BALF samples and also to significantly decrease MMP-9 level ($p \leq 0.05$) matches its superiority in improving pulmonary function. It also matches the biochemical results showing its superior anti-inflammatory and antioxidant effects.

3.5.7. Lung histopathological changes

To further confirm the results obtained, histopathological examination of H&E-stained lung tissue sections was done (Fig. 9). Negative control rats revealed the classical structure of normal lung with patent clear bronchial and alveolar spaces and thin alveolar septa. On the other hand, untreated ALI positive control rats' samples revealed severe disturbance of lung architecture with extensive areas of consolidation and collapsed alveoli with extensive cellular infiltration. The remnant alveoli mostly showed thickened alveolar septa, degenerative lining cells and intraluminal cellular debris which appeared also on bronchiolar lumina. Alveoli with empty lumina and thin alveolar septa were rarely seen. An eosinophilic exudate was occasionally seen within the cellular infiltration. TSIIA suspension partially alleviated the pathological changes with reappearance of considerable areas of patent alveoli with either thin or thick interalveolar septa. Localized areas of hyalinized eosinophilic material surrounded by intense monocellular infiltration were commonly seen. Lung samples obtained from NE-F8 treated group revealed partial improvement with evident peribronchiolar mononuclear cellular infiltration and collapsed alveoli. Moreover, administration of TSIIA-NE-F8 nearly relieved most of the pathological changes, but groups of narrow alveoli with intraluminal cellular debris were still encountered.

The superior physiological, biochemical, and histopathological effects of TSIIA-NE-F8 compared to TSIIA suspension could be ascribed to the ability of the nano-formulation to permit targeted drug delivery to

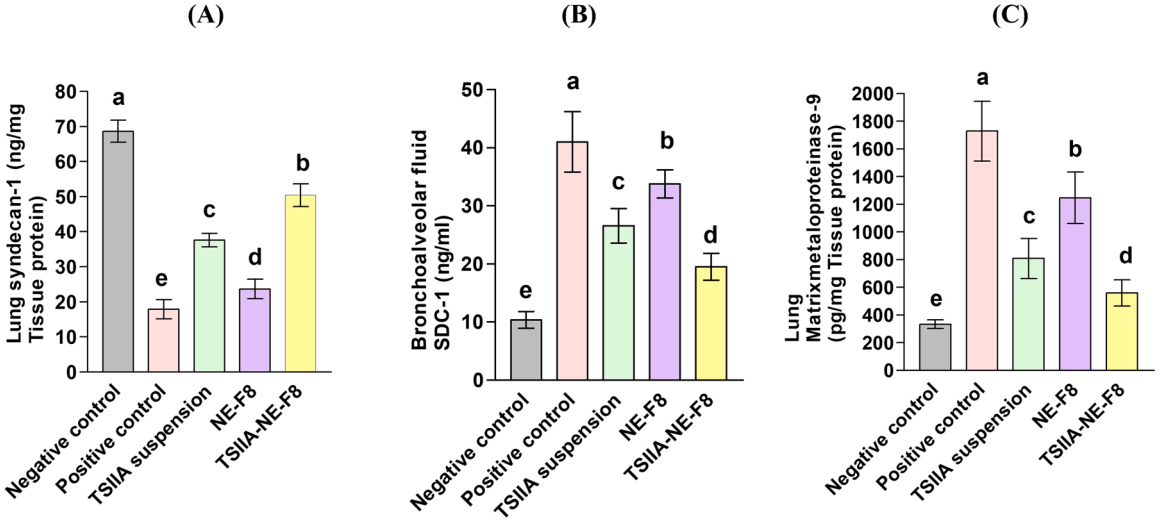

Fig. 8. Effect of different formulations and TSIIA suspension on endothelial glycocalyx shedding markers; **(A)** Lung syndecan-1, **(B)** BALF syndecan-1 and **(C)** Lung MMP-9 after a single dose (30 μg/kg) intratracheal administration to an LPS -induced ALI rat model. Data were expressed as means ± SD (n = 7). Data were analyzed using one-way ANOVA followed by post hoc test (Duncan) for group comparisons. Means of similar symbols were statistically insignificant: a > b > c > d > e ($p \leq 0.05$).

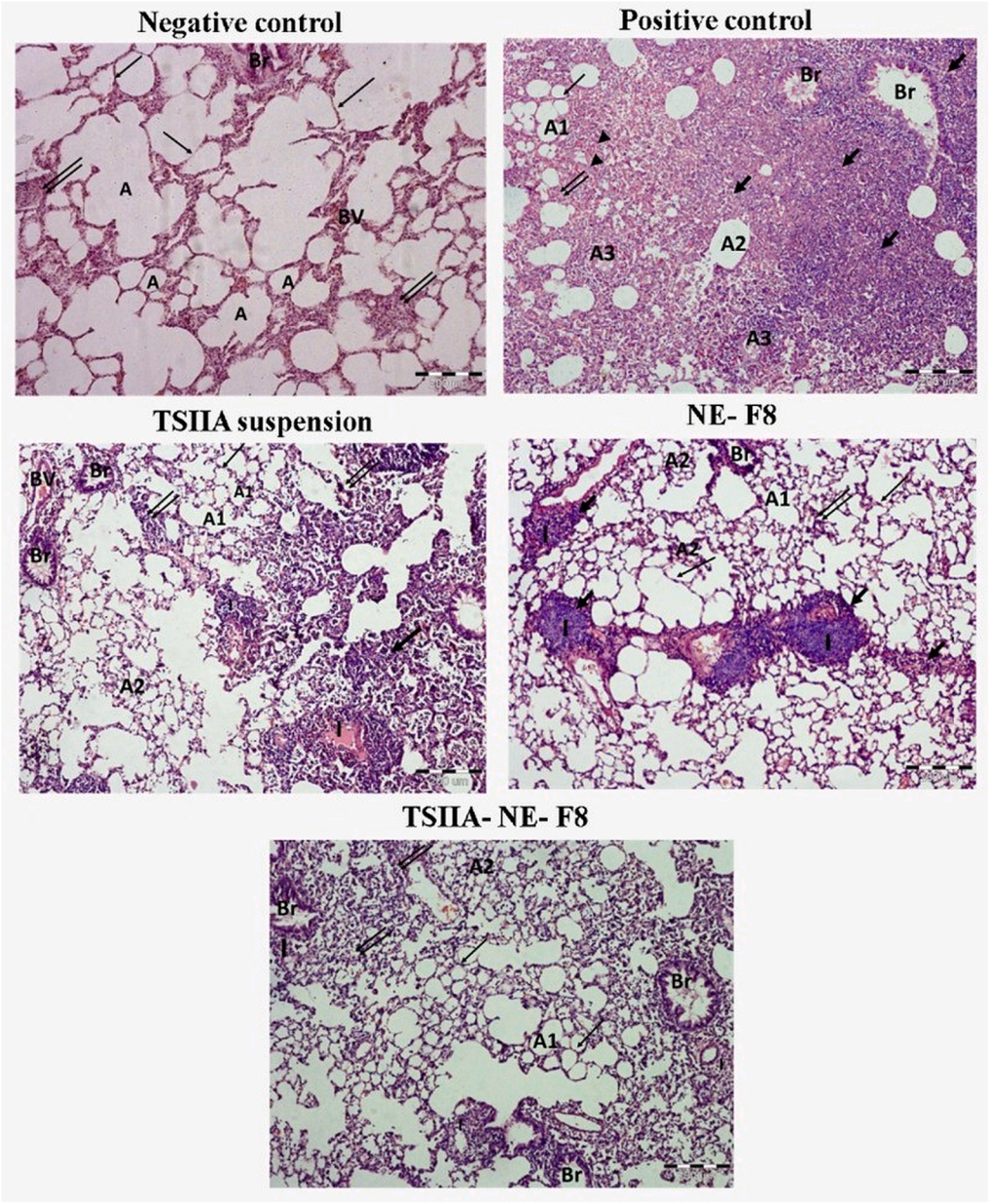

Fig. 9. Histopathological photomicrographs of H & E stained lung tissue sections of: **Negative control** showing normal alveolar spaces **(A)** with thin alveolar septa (**thin arrow**). **Positive control** with evident consolidation and cellular infiltration **(thick arrow)**. The remnant alveoli depicted different features. Some were patent **(A1)** with thin (**thin arrow**) or thick **(double arrow)** alveolar septa. Others showed degeneration **(A2)**. Intraluminal exudate and cellular debris are seen in the bronchiole **(Br)** and some alveoli **(A3)**. Eosinophilic infiltration and exudate are occasionally seen **(arrowhead). TSIIA suspension, NE-F8 and TSIIA-NE-F8 groups** show improved lung condition, many alveoli are patent **(A1)** with thin alveolar septa (**thin arrow)** or slightly thickened ones **(double arrow)**. Groups of narrow collapsed degenerated alveoli **(A2)** with intracellular debris are also seen. Notice the marked improvement in **TSIIA-NE-F8** section**.** While in **TSIIA suspension & NE-F8 groups**, still there are widened consolidated areas **(thick arrow)** more prevalent in **NE-F8 group.** Both **TSIIA suspension & NE-F8 groups** also show peribronchiolar & localized cellular infiltration **(I)** surrounding an eosinophilic hyalinized materials that are also more evident in **NE-F8 group**. Scale bar represents 200 μm.

lung tissues for a longer period with greater ability to successfully penetrate through the lungs. Chattopadhyay et al. [82] similarly explained the improved efficacy for inhalable atropine polymeric nanoparticles in amelioration of airway hyperreactivity and remodeling in a murine model of chronic asthma compared to free drug. The effectiveness of TSIIA-NE-F8 could also be attributed to the use of biologically active ingredients with anti-inflammatory and anti-oxidant activities thus augmenting drug activity.

4. Conclusion

Herein, for the first time, a NE based on bioactive ingredients for the pulmonary delivery of TSIIA was tailored and its efficacy in the management of LPS-induced ALI rat model was evaluated versus either free drug suspension or blank NE. A simple method of preparation was adopted. The developed NE offered several advantages, including the use of safe, biocompatible and bioactive excipients. Formulation selection was based on optimum colloidal properties and entrapment efficiency. The mechanistic study demonstrated the protective effect of TSIIA on a key factor and an important therapeutic target in the treatment of ALI; glycocalyx degradation and shedding. The observed effect may be due to its well reported antioxidant anti-inflammatory actions that can affect glycocalyx enzymatic degradation. This effect was further augmented by drug loading into NE probably due to the innate pharmacological activity of TTO and rhamnolipid and the enhanced in vivo performance of nanoformulations. Our findings possibly offer a new platform for the treatment of ALI through decreasing endothelial dysfunction and vascular leakage.

Disclosure

The authors report no conflicts of interest in this work.

CRediT authorship contribution statement

Riham M. El-Moslemany: Conceptualization, Data curation, Formal

analysis, Funding acquisition, Investigation, Methodology, Project administration, Resources, Visualization, Writing – original draft, Writing – review & editing. **Amal H. El-Kamel:** Conceptualization, Data curation, Formal analysis, Funding acquisition, Resources, Supervision, Writing – review & editing. **Eman A. Allam:** Data curation, Formal analysis, Funding acquisition, Investigation, Methodology, Resources, Software, Writing – original draft, Writing – review & editing. **Hoda M. Khalifa:** Data curation, Formal analysis, Investigation, Visualization. **Ahmed Hussein:** Methodology, Validation, Visualization, Writing – original draft. **Asmaa A. Ashour:** Conceptualization, Data curation, Formal analysis, Funding acquisition, Investigation, Methodology, Resources, Software, Validation, Visualization, Writing – original draft, Writing – review & editing.

Conflict of Interest

Authors declare no conflicts of interest.

Appendix A. Supporting information

Supplementary data associated with this article can be found in the online version at doi:10.1016/j.biopha.2022.113666.

References

[1] H. Okada, S. Yoshida, A. Hara, S. Ogura, H. Tomita, Vascular endothelial injury exacerbates coronavirus disease 2019: the role of endothelial glycocalyx protection, Microcirculation 28 (3) (2021), e12654.

[2] X. Chen, X. Zhang, J. Zhang, Y. Gao, Z. Yang, S. Li, H. Dai, Attenuation of acute lung injury in a rat model by Semen Cassiae, BMC Complement. Altern. Med. 17 (1) (2017) 234–240.

[3] R. Blondonnet, J.M. Constantin, V. Sapin, M. Jabaudon, A. Pathophysiologic, Approach to biomarkers in acute respiratory distress syndrome, Dis. Mark. 2016 (2016), 3501373.

[4] T. Iba, J.H. Levy, T. Hirota, M. Hiki, K. Sato, T. Murakami, I. Nagaoka, Protection of the endothelial glycocalyx by antithrombin in an endotoxin-induced rat model of sepsis, Thromb. Res. 171 (2018) 1–6.

[5] R. Uchimido, E.P. Schmidt, N.I. Shapiro, The glycocalyx: a novel diagnostic and therapeutic target in sepsis, Crit. Care 23 (1) (2019) 16–28.

[6] D. Zhang, B.Y. Qi, W.W. Zhu, X. Huang, X.Z. Wang, Crocin alleviates lipopolysaccharide-induced acute respiratory distress syndrome by protecting against glycocalyx damage and suppressing inflammatory signaling pathways, Inflamm. Res. 69 (3) (2020) 267–278.

[7] B.F. Becker, M. Jacob, S. Leipert, A.H. Salmon, D. Chappell, Degradation of the endothelial glycocalyx in clinical settings: searching for the sheddases, Br. J. Clin. Pharm. 80 (3) (2015) 389–402.

[8] T.M. Reine, F. Lanzalaco, O. Kristiansen, A.R. Enget, S. Satchell, T.G. Jenssen, S. O. Kolset, Matrix metalloproteinase-9 mediated shedding of syndecan-4 in glomerular endothelial cells, Microcirculation (2019), e12534.

[9] T. Parimon, C. Yao, D.M. Habiel, L. Ge, S.A. Bora, R. Brauer, C.M. Evans, T. Xie, F. Alonso-Valenteen, L.K. Medina-Kauwe, D. Jiang, P.W. Noble, C.M. Hogaboam, N. Deng, O. Burgy, T.J. Antes, M. Königshoff, B.R. Stripp, S.A. Gharib, P. Chen, Syndecan-1 promotes lung fibrosis by regulating epithelial reprogramming through extracellular vesicles, JCI Insight 5 (17) (2019), e129359.

[10] Z. Zhang, N. Chen, J.B. Liu, J.B. Wu, J. Zhang, Y. Zhang, X. Jiang, Protective effect of resveratrol against acute lung injury induced by lipopolysaccharide via inhibiting the myd88-dependent Toll-like receptor 4 signaling pathway, Mol. Med. Rep. 10 (1) (2014) 101–106.

[11] A.A. Ashour, A.A. Ramadan, D.A. Abdelmonsif, A.H. El-Kamel, Enhanced oral bioavailability of Tanshinone IIA using lipid nanocapsules: formulation, in-vitro appraisal and pharmacokinetics, Int. J. Pharm. 586 (2020), 119598.

[12] S. Mao, L. Wang, P. Chen, Y. Lan, R. Guo, M. Zhang, Nanoparticle-mediated delivery of Tanshinone IIA reduces adverse cardiac remodeling following myocardial infarctions in a mice model: role of NF-κB pathway, Artif. Cells Nanomed. Biotechnol. 46 (sup3) (2018) S707–S716.

[13] M. Xu, F. Cao, L. Liu, B. Zhang, Y. Wang, H. Dong, Y. Cui, M. Dong, D. Xu, Y. Liu, P. Zhao, W. Niu, Z. Li, Tanshinone IIA-induced attenuation of lung injury in endotoxemic mice is associated with reduction of hypoxia-inducible factor 1α expression, Am. J. Respir. Cell Mol. Biol. 45 (5) (2011) 1028–1035.

[14] M. Xu, F.L. Cao, Y.F. Zhang, L. Shan, X.L. Jiang, X.J. An, W. Xu, X.Z. Liu, X. Y. Wang, Tanshinone IIA therapeutically reduces LPS-induced acute lung injury by inhibiting inflammation and apoptosis in mice, Acta Pharm. Sin. 36 (2) (2015) 179–187.

[15] A.A. Ashour, A.H. El-Kamel, D.A. Abdelmonsif, H.M. Khalifa, A.A. Ramadan, Modified lipid nanocapsules for targeted tanshinone IIA delivery in liver fibrosis, Int. J. Nanomed. 16 (2021) 8013–8033.

[16] J. Lin, X. Wang, Q. Wu, J. Dai, H. Guan, W. Cao, L. He, Y. Wang, Development of Salvianolic acid B-Tanshinone II A-Glycyrrhetinic acid compound liposomes: formulation optimization and its effects on proliferation of hepatic stellate cells, Int. J. Pharm. 462 (1–2) (2014) 11–18.

[17] W.L. Zhang, J.P. Liu, X.X. Liu, Z.Q. Chen, Stealth tanshinone IIA-loaded solid lipid nanoparticles: effects of poloxamer 188 coating on in vitro phagocytosis and in vivo pharmacokinetics in rats, Yao Xue Xue Bao 44 (12) (2009) 1421–1428.

[18] H. Ma, Q. Fan, J. Yu, J. Xin, C. Zhang, Novel microemulsion of tanshinone IIA, isolated from Salvia miltiorrhiza Bunge, exerts anticancer activity through inducing apoptosis in hepatoma cells, Am. J. Chin. Med. 41 (1) (2013) 197–210.

[19] L.C. Chang, C.L. Wu, C.W. Liu, W.H. Chuo, P.C. Li, T.R. Tsai, Preparation, characterization and cytotoxicity evaluation of tanshinone IIA nanoemulsions, J. Biomed. Nanotechnol. 7 (4) (2011) 558–567.

[20] J. Zhang, Y. Li, X. Fang, D. Zhou, Y. Wang, M. Chen, TPGS-g-PLGA/Pluronic F68 mixed micelles for tanshinone IIA delivery in cancer therapy, Int. J. Pharm. 476 (1–2) (2014) 185–198.

[21] M. Jaiswal, R. Dudhe, P.K. Sharma, Nanoemulsion: an advanced mode of drug delivery system, 3 Biotech 5 (2) (2015) 123–127.

[22] S. Ganta, M. Talekar, A. Singh, T.P. Coleman, M.M. Amiji, Nanoemulsions in translational research-opportunities and challenges in targeted cancer therapy, AAPS PharmSciTech 15 (3) (2014) 694–708.

[23] C. Zhao, J. Sun, C. Fang, F. Tang, 1,8-cineol attenuates LPS-induced acute pulmonary inflammation in mice, Inflammation 37 (2) (2014) 566–572.

[24] M. Asif, M. Saleem, M. Saadullah, H.S. Yaseen, R. Al Zarzour, COVID-19 and therapy with essential oils having antiviral, anti-inflammatory, and immunomodulatory properties, Inflammopharmacology 28 (5) (2020) 1153–1161.

[25] M. Wan, Y.F. Yao, W. Wu, W.W. Fu, R.T. Wu, W.J. Li, Chimonanthus nitens Oliv. essential oil mitigates lipopolysaccharide-induced acute lung injury in rats, Food Chem. Toxicol. 156 (2021), 112445.

[26] G. Ramage, S. Milligan, D.F. Lappin, L. Sherry, P. Sweeney, C. Williams, J. Bagg, S. Culshaw, Antifungal, cytotoxic, and immunomodulatory properties of tea tree oil and its derivative components: potential role in management of oral candidosis in cancer patients, Front. Microbiol. 3 (2012) 220–228.

[27] M. Golab, K. Skwarlo-Sonta, Mechanisms involved in the anti-inflammatory action of inhaled tea tree oil in mice, Exp. Biol. Med. 232 (3) (2007) 420–426.

[28] M.M. Abdellatif, Y.E. Elakkad, A.A. Elwakeel, R.M. Allam, M.R. Mousa, Formulation and characterization of propolis and tea tree oil nanoemulsion loaded with clindamycin hydrochloride for wound healing: in-vitro and in-vivo wound healing assessment, Saudi Pharm. J. 29 (11) (2021) 1238–1249.

[29] A. Wulansari, M. Jufri, A. Budianti, Studies on the formulation, physical stability, and in vitro antibacterial activity of tea tree oil (Melaleuca alternifolia) nanoemulsion gel, Int. J. Appl. Pharmaceut. 9 (1) (2017) 135–139.

[30] P. Thakur, N.K. Saini, V.K. Thakur, V.K. Gupta, R.V. Saini, A.K. Saini, Rhamnolipid the glycolipid biosurfactant: emerging trends and promising strategies in the field of biotechnology and biomedicine, Microb. Cell Fact. 20 (1) (2021) 1–15.

[31] M.D. Subramaniam, D. Venkatesan, M. Iyer, S. Subbarayan, V. Govindasami, A. Roy, A. Narayanasamy, S. Kamalakannan, A.V. Gopalakrishnan, R. Thangarasu, N.S. Kumar, B. Vellingiri, Biosurfactants and anti-inflammatory activity: a potential new approach towards COVID-19, Curr. Opin. Environ. Sci. Health 17 (2020) 72–81.

[32] N. Ahmad, R. Ahmad, A. Al-Qudaihi, S.E. Alaseel, I.Z. Fita, M.S. Khalid, F. H. Pottoo, Preparation of a novel curcumin nanoemulsion by ultrasonication and its comparative effects in wound healing and the treatment of inflammation, RSC Adv. 9 (35) (2019) 20192–20206.

[33] S. Wei, X. Zhao, J. Yu, S. Yin, M. Liu, R. Bo, J. Li, Characterization of tea tree oil nanoemulsion and its acute and subchronic toxicity, Regul. Toxicol. Pharm. 124 (2021), 104999.

[34] Y. Zhang, M. Huo, J. Zhou, A. Zou, W. Li, C. Yao, S. Xie, DDSolver: an add-in program for modeling and comparison of drug dissolution profiles, AAPS J. 12 (3) (2010) 263–271.

[35] O. Westphal, Bacterial lipopolysaccharides extraction with phenol-water and further applications of the procedure, Methods Carbohydr. Chem. 5 (1965) 83–91.

[36] X. Wu, Q. Kong, Z. Xia, L. Zhan, W. Duan, X. Song, Penehyclidine hydrochloride alleviates lipopolysaccharide-induced acute lung injury in rats: potential role of caveolin-1 expression upregulation, Int. J. Mol. Med. 43 (5) (2019) 2064–2074.

[37] L. Li, Y.G. Zhang, Y.F. Tan, J.J. Zhao, H.R. Zhang, B. Zhao, Tanshinone II is a potent candidate for treatment of lipopolysaccharide-induced acute lung injury in rat model, Oncol. Lett. 15 (2) (2018) 2550–2554.

[38] N. Limjunyawong, W. Mitzner, M.R. Horton, A mouse model of chronic idiopathic pulmonary fibrosis, Physiol. Rep. 2 (2) (2014), e00249.

[39] B. Li, Q. Lin, Q. Hou, C. Yin, L. Zhang, Y. Li, Alkannin attenuates lipopolysaccharide-induced lung injury in mice via Rho/ROCK/NF-κB pathway, J. Biochem. Mol. Toxicol. 33 (7) (2019), e22323.

[40] S. Kumar, P. Bhagat, S.C. Patne, R. Pandey, Role of insulin in oleic acid-induced acute lung injury in rat model, IJPP 65 (2) (2021) 103–108.

[41] O.H. Lowry, N.J. Rosebrough, A.L. Farr, R.J. Randall, Protein measurement with the Folin phenol reagent, J. Biol. Chem. 193 (1) (1951) 265–275.

[42] H. Ohkawa, N. Ohishi, K. Yagi, Assay for lipid peroxides in animal tissues by thiobarbituric acid reaction, Anal. Biochem. 95 (2) (1979) 351–358.

[43] S. Marklund, G. Marklund, Involvement of the superoxide anion radical in the autoxidation of pyrogallol and a convenient assay for superoxide dismutase, Eur. J. Biochem. 47 (3) (1974) 469–474.

[44] D.E. Paglia, W.N. Valentine, Studies on the quantitative and qualitative characterization of erythrocyte glutathione peroxidase, J. Lab. Clin. Med. 70 (1) (1967) 158–169.

[45] M.K. Al-Sakkaf, S.A. Onaizi, Rheology, characteristics, stability, and pH-responsiveness of biosurfactant-stabilized crude oil/water nanoemulsions, Fuel 307 (2022), 121845.

[46] N.P. Nirmal, R. Mereddy, L. Li, Y. Sultanbawa, Formulation, characterisation and antibacterial activity of lemon myrtle and anise myrtle essential oil in water nanoemulsion, Food Chem. 254 (2018) 1–7.
[47] N. Ahmad, R. Ahmad, A. Al-Qudaihi, S.E. Alaseel, I.Z. Fita, M.S. Khalid, F. H. Pottoo, Preparation of a novel curcumin nanoemulsion by ultrasonication and its comparative effects in wound healing and the treatment of inflammation, RSC Adv. 9 (35) (2019) 20192–20206.
[48] H.H. Ali, A.A. Hussein, Oral nanoemulsions of candesartan cilexetil: formulation, characterization and in vitro drug release studies, AAPS Open 3 (1) (2017) 4–19.
[49] S. Uppal, P. Sharma, R. Kumar, K. Kaur, A. Bhatia, S.K. Mehta, Effect of benzyl isothiocyanate encapsulated biocompatible nanoemulsion prepared via ultrasonication on microbial strains and breast cancer cell line MDA MB 231, Colloids Surf. A Physicochem. Eng. Asp. 596 (2020), 124732.
[50] J.P. Gokhale, H.S. Mahajan, S.J. Surana, Quercetin loaded nanoemulsion-based gel for rheumatoid arthritis: in vivo and in vitro studies, Biomed. Pharmacother. 112 (2019), 108622.
[51] N.H. Arbain, N. Salim, H.R.F. Masoumi, T.W. Wong, M. Basri, M.B. Abdul Rahman, In vitro evaluation of the inhalable quercetin loaded nanoemulsion for pulmonary delivery, Drug Deliv. Transl. Res. 9 (2) (2019) 497–507.
[52] A.P. Silva, B.R. Nunes, M.C. De Oliveira, L.S. Koester, P. Mayorga, V.L. Bassani, H. F. Teixeira, Development of topical nanoemulsions containing the isoflavone genistein, Pharmazie 64 (1) (2009) 32–35.
[53] H. Domscheit, M.A. Hegeman, N. Carvalho, P.M. Spieth, Molecular dynamics of lipopolysaccharide-induced lung injury in rodents, Front. Physiol. 11 (2020) 36–43.
[54] H. Chen, C. Bai, X. Wang, The value of the lipopolysaccharide-induced acute lung injury model in respiratory medicine, Expert Rev. Respir. Med. 4 (6) (2010) 773–783.
[55] B. Ijaz, A. Shabbir, M. Shahzad, A. Mobashar, M. Sharif, M.I. Basheer, R.B. Tareen, N.I. Syed, Amelioration of airway inflammation and pulmonary edema by Teucrium stocksianum via attenuation of pro-inflammatory cytokines and up-regulation of AQP1 and AQP5, Respir. Physiol. Neurobiol. 284 (2021), 103569.
[56] Z. Cao, J.-L. Liu, S. Wu, Q. Wang, Mechanism of MCP-1 in acute lung injury and advanced therapy by drug-loaded dextrin nanoparticle, Int. J. Polym. Sci. 2018 (2018).
[57] Y. Wang, H. Wu, W. Niu, J. Chen, M. Liu, X. Sun, Z. Li, Tanshinone IIA attenuates paraquat-induced acute lung injury by modulating angiotensin-converting enzyme 2/angiotensin-(1-7) in rats, Mol. Med. Rep. 18 (3) (2018) 2955–2962.
[58] R. Zhang, X. Shi, Y. Chen, J. Liu, Y. Wu, Y. Xu, Multi-omics revealed the protective effects of rhamnolipids in lipopolysaccharide challenged broilers, Front. Immunol. 13 (2022), 824664.
[59] J. Ning, L. Xu, Q. Zhao, Y.Y. Zhang, C.Q. Shen, The protective effects of terpinen-4-ol on LPS-induced acute lung injury via activating PPAR-γ, Inflammation 41 (6) (2018) 2012–2017.
[60] X. Huang, H. Xiu, S. Zhang, G. Zhang, The role of macrophages in the pathogenesis of ALI/ARDS, Mediat. Inflamm. 2018 (2018), 1264913.
[61] G. Fan, X. Jiang, X. Wu, P.A. Fordjour, L. Miao, H. Zhang, Y. Zhu, X. Gao, Anti-inflammatory activity of tanshinone IIA in LPS-stimulated RAW264.7 macrophages via miRNAs and TLR4-NF-κB pathway, Inflammation 39 (1) (2016) 375–384.
[62] X.Y. Qin, T. Li, L. Yan, Q.S. Liu, Y. Tian, Tanshinone IIA protects against immune-mediated liver injury through activation of T-cell subsets and regulation of cytokines, Immunopharmacol. Immunotoxicol. 32 (1) (2010) 51–55.
[63] J. Yan, X. Yang, D. Han, J. Feng, Tanshinone IIA attenuates experimental autoimmune encephalomyelitis in rats, Mol. Med. Rep. 14 (2) (2016) 1601–1609.
[64] N. Pazyar, R. Yaghoobi, N. Bagherani, A. Kazerouni, A review of applications of tea tree oil in dermatology, Int. J. Dermatol. 52 (7) (2013) 784–790.
[65] C. Salvatori, L. Barchi, F. Guzzo, M. Gargari, A comparative study of antibacterial and anti-inflammatory effects of mouthrinse containing tea tree oil, Oral Implantol. 10 (1) (2017) 59–70.
[66] P. Hart, C. Brand, C. Carson, T. Riley, R. Prager, J. Finlay-Jones, Terpinen-4-ol, the main component of the essential oil of Melaleuca alternifolia (tea tree oil), suppresses inflammatory mediator production by activated human monocytes, Inflamm. Res. 49 (11) (2000) 619–626.
[67] R. Kumar, A.J. Das, Application of rhamnolipids in medical sciences, Rhamnolipid Biosurfactant, Springer, 2018, pp. 79–87.
[68] Z. Dong, Y. Yuan, Accelerated inflammation and oxidative stress induced by LPS in acute lung injury: Inhibition by ST1926, Int. J. Mol. Med. 41 (6) (2018) 3405–3421.
[69] D.P. Dos Santos Haupenthal, C. Mendes, G. de Bem Silveira, R.P. Zaccaron, M. Corrêa, R.T. Nesi, R.A. Pinho, M.M. da Silva Paula, P.C.L. Silveira, Effects of treatment with gold nanoparticles in a model of acute pulmonary inflammation induced by lipopolysaccharide, J. Biomed. Mater. Res. A 108 (1) (2020) 103–115.
[70] J. Zhou, Z. Peng, J. Wang, Trelagliptin alleviates lipopolysaccharide (LPS)-induced inflammation and oxidative stress in acute lung injury mice, Inflammation 44 (4) (2021) 1507–1517.
[71] R. Huang, T. Zhong, H. Wu, Quercetin protects against lipopolysaccharide-induced acute lung injury in rats through suppression of inflammation and oxidative stress, Arch. Med. Sci. 11 (2) (2015) 427–432.
[72] S.-B. Wang, X.-F. Guo, B. Weng, S.-P. Tang, H.-J. Zhang, Tanshinone IIA attenuates ovalbumin-induced airway inflammation and hyperresponsiveness in a murine model of asthma, Iran J. Basic Med. Sci. 22 (2) (2019) 160–165.
[73] N. Puvača, I. Čabarkapa, V. Bursić, A. Petrović, M. Aćimović, Antimicrobial, antioxidant and acaricidal properties of tea tree (Melaleuca alternifolia), J. Agron. Technol. Eng. Manag. 1 (1) (2018) 29–38.
[74] R.S. AlRazn, Z.R. AbdulHussein, Biological effect of rhamnolipid as antioxidant and anticancer agent, Ann. Rom. Soc. Cell Biol. 25 (6) (2021) 1744–1758.
[75] M. Qin, Z. Qiu, Changes in TNF-α, IL-6, IL-10 and VEGF in rats with ARDS and the effects of dexamethasone, Exp. Ther. Med. 17 (1) (2019) 383–387.
[76] Y. Yang, E.P. Schmidt, The endothelial glycocalyx: an important regulator of the pulmonary vascular barrier, Tissue Barriers 1 (1) (2013), e23494.
[77] S. Weidenfeld, W.M. Kuebler, Shedding first light on the alveolar epithelial glycocalyx, Am. J. Respir. Cell Mol. Biol. 59 (3) (2018) 283–284.
[78] X.Y. Liu, H.X. Xu, J.K. Li, D. Zhang, X.H. Ma, L.N. Huang, J.H. Lü, X.Z. Wang, Neferine protects endothelial glycocalyx via mitochondrial ROS in lipopolysaccharide-induced acute respiratory distress syndrome, Front. Physiol. 9 (2018) 102–115.
[79] H. Kolářová, B. Ambrůzová, L. Svihálková Šindlerová, A. Klinke, L. Kubala, Modulation of endothelial glycocalyx structure under inflammatory conditions, Mediat. Inflamm. 2014 (2014), 694312.
[80] C. Chelazzi, G. Villa, P. Mancinelli, A.R. De Gaudio, C. Adembri, Glycocalyx and sepsis-induced alterations in vascular permeability, Crit. Care 19 (1) (2015) 26–32.
[81] L. Chen, W. Li, D. Qi, D. Wang, Lycium barbarum polysaccharide protects against LPS-induced ARDS by inhibiting apoptosis, oxidative stress, and inflammation in pulmonary endothelial cells, Free Radic. Res. 52 (4) (2018) 480–490.
[82] P. Chattopadhyay, M.P. Pathak, P. Patowary, S. Chakrabarti, D. Goyary, S. Karmakar, S.K. Dwivedi, Synthesized atropine nanoparticles ameliorate airway hyperreactivity and remodeling in a murine model of chronic asthma, J. Drug Deliv. Sci. Technol. 56 (2020), 101507.